JACS
JOURNAL OF THE AMERICAN CHEMICAL SOCIETY
Article
pubs.acs.org/JACS

Ultrafast Structural Dynamics Inside Planar Phospholipid Multibilayer Model Cell Membranes Measured with 2D IR Spectroscopy

Oksana Kel, Amr Tamimi, Megan C. Thielges,[#] and Michael D. Fayer*

Department of Chemistry, Stanford University, Stanford, California 94305, United States

ABSTRACT: The ultrafast dynamics in the interior of planar aligned multibilayers of 1,2-dilauroyl-*sn*-glycero-3-phosphocholine (dilauroylphosphatidylcholine, DLPC) are investigated using 2D IR vibrational echo spectroscopy. The nonpolar and water insoluble vibrational dynamics probe, tungsten hexacarbonyl ($W(CO)_6$), is located in the alkane interior of the membranes. The 2D IR experiments conducted on the antisymmetric CO stretching mode measure spectral diffusion caused by the structural dynamics of the membrane from ~200 fs to ~200 ps as a function of the number of water molecules hydrating the head groups and as a function of cholesterol content for a fixed hydration level. FT-IR studies of the lipid bilayers and the model liquids, hexadecane and bis(2-ethylhexyl) succinate, indicate that as the number of hydrating water molecules increases from 2 to 16, there are structural changes in the membrane that partition some of the $W(CO)_6$ into the ester region of DLPC. However, the 2D IR measurements, which are made solely on the $W(CO)_6$ in the alkane regions, show that the level of hydration has no observable impact on the interior membrane dynamics. FT-IR spectra and 2D IR experiments on samples with cholesterol concentrations from 0 to 60% demonstrate that there is a change in the membrane structure and an abrupt change in dynamics at 35% cholesterol. The dynamics are independent of cholesterol content from 10 to 35%. At 35%, the dynamics become slower and remain unchanged from 35 to 60% cholesterol.

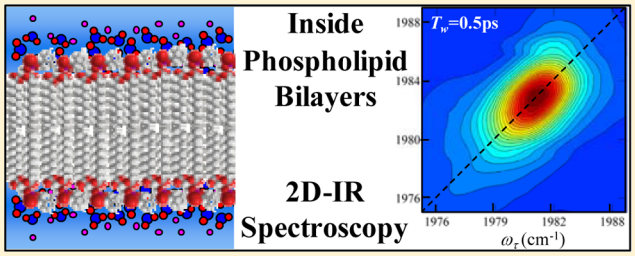

I. INTRODUCTION

The plasma membrane provides a boundary between a living cell and its surroundings enabling organizational control of proteins, small molecules, and ion localization that is critical to the complexity of biological systems. In addition to a permeability barrier, the second role of membranes is to serve as the "solvent" for membrane proteins and other molecules located in membranes or that pass through membranes. The lipid environment of proteins influences their function,[1−5] and so impact cell signaling, metabolism, growth, defense, and a myriad of other biological functions.

The plasma membrane is a nanoscale collective structure primarily composed of phospholipids, embedded proteins, and other molecules, such as cholesterol.[6,7] Biological membranes have a highly organized bilayer structure due to their amphiphilic nature. The nonpolar alkane chains of the phospholipids form the interior of a molecular bilayer, with zwitterionic or ionic head groups at the interfaces with water. The lipid compositions can vary and lead to differences in the physical properties of the membranes.[1,7] Eukaryotic membranes tend to have neutral lipids with zwitterionic head groups such as phosphatidylcholine and sphingomyelin, as well sterols like cholesterol.

Cholesterol is an important component of many plasma membranes where it is found in concentrations that can be greater than 25%,[8] although in mitochondrial and endoplasmic reticulum membranes it is less than 5%. Cholesterol has a substantial impact on the structural properties of membranes. The area of phospholipids in the bilayer decreases with increasing cholesterol concentration.[9] Also, the presence of cholesterol influences the mechanical properties of membranes.[10] Its presence leads to a decrease in the enthalpy of the lipid bilayers gel to liquid−crystalline phase transition and keeps membranes in a more fluid liquid−crystalline phase.[10−13]

Because of the importance of biological membranes, a variety of biophysical techniques, such as fluorescence microscopy, atomic force microscopy, and visible and vibrational spectroscopy, are used to investigate their structure and heterogeneity.[14−20] Dynamic properties and membrane phase transition behavior have been extensively studied by EPR and NMR spectroscopy.[21−29] Analysis of line shape changes with, e.g., changing temperature or cholesterol concentration provides order parameters and rotational diffusion rates of the lipids, which generally occur in the range 10^9−10^7 s^{-1}.[30,31] Also, the oxygen and other paramagnetic molecules transport parameters across lipid bilayers have been used to characterize the dynamics of bilayers.[25,32] The time scale of the transport process is in the μs region. Very high frequency EPR line shape analysis has been employed to examine the temperature

Received: March 23, 2013
Revised: April 12, 2013
Published: July 9, 2013

   dx.doi.org/10.1021/ja403675x | *J. Am. Chem. Soc.* 2013, 135, 11063−11074

dependent 100 ps time scale orientational relaxation of a small probe molecule in vesicle bilayers.[33]

Here the ultrafast structural dynamics of the interior alkane regions of membranes and how interior membrane dynamics are affected by cholesterol and the degree of headgroup hydration are investigated. Ultrafast two-dimensional infrared (2D IR) vibrational echo experiments[34,35] and IR pump−probe experiments[36] are employed to address structural dynamics on the time scales of 200 fs to 200 ps. Previously, 2D IR experiments have been used to investigate transmembrane peptides by analyzing the multiple peaks in the amide I band spectrum of the peptide backbone,[37−40] and biomolecules bound to membranes.[41] These experiments and simulations provide information on the biomolecular structure but do not examine the time dependence of the systems.[37−41] IR pump−probe vibrational lifetime measurements of a probe molecule in phospholipid multibilayer have been used to observe distinct locations for the probe and changing levels of hydration.[42]

Chemistry depends to a great extent the solvent, which provides dynamical intermolecular interactions that are intimately involved in chemical processes. For cytosolic proteins and enzymes, the medium is water. MD simulations use sophisticated water models that do a reasonable job of reproducing the dynamics of water's mechanical degrees of freedom. The bath degrees of freedom can be included in these MD simulations because there is a broad understanding of water dynamics, and water simulations have been tested against experiments, principally ultrafast 2D IR vibrational echo experiments.[43−46] Our knowledge of the ultrafast internal structural dynamics of membranes, which serve as the bath modes for membrane processes, is almost nonexistent by comparison to what we know about water.

Important insights have been gained by multiple methods that address slower time scale dynamics. For example, translational diffusion of lipids and cholesterol is intimately involved in the formation of rafts and the motion of transmembrane proteins. Ultrafast membrane structural dynamics give rise to the slower time scale macroscopic motions, but they also play other roles. The ultrafast dynamics of the membrane bath are directly connected to the structural fluctuations of transmembrane proteins and other membrane biomolecules. Motions of the solvent (membrane) drive structural changes of the protein. In addition, for the internal structure of a protein to change, generally there will be some structural change at the protein surface. The internal motions of a transmembrane protein are tied to the ability of the membrane structure to respond by accommodating the proteins shape changes, and membrane structural fluctuations to induce protein structural fluctuations.[47] The ultrafast membrane structural dynamics are a spectrum of response times. Protein structural changes that are matched to the response times are facilitated. In addition, the ultrafast membrane dynamics provide the structural fluctuations that permit relatively small molecules to move in and through membranes in a manner analogous to a solute moving through a normal solvent.

To study ultrafast membrane dynamics, 2D IR vibrational echo and IR pump−probe experiments as well as FT-IR absorption studies are performed on the antisymmetric CO stretching mode of the vibrational probe molecule, $W(CO)_6$, in aligned multibilayers of 1,2-dilauroyl-*sn*-glycero-3-phosphocholine (dilauroylphosphatidylcholine, DLPC). DLPC has been studied extensively using many techniques in the context of understanding membrane structure, dynamics, and the properties of proteins and other biomolecules located in membranes.[48−61] $W(CO)_6$, which is nonpolar and insoluble in water, dissolves in the interiors of the DLPC bilayers. The 2D IR vibrational echo experiments[34,35] measure spectral diffusion, which is caused by the structural evolution of the interior of the bilayers. Because $W(CO)_6$ has a long vibrational lifetime, the dynamics can be measured from ∼200 fs to ∼200 ps, which is sufficient to observe the full range of ultrafast structural fluctuations of the membrane's interior. The measurements are performed as a function of the number of water molecules solvating the zwitterionic head groups, with the number of water molecules ranging from 2 to 16. Previous studies examined the dynamics of the water between the bilayers.[62−66] In addition, the dynamics are studied as a function of cholesterol content of the bilayers. The cholesterol concentration ranges from 0 to 60%. Comparisons are made to two model liquids, hexadecane and bis(2-ethylhexyl) succinate (EHS).

The FT-IR studies as a function of water content indicate that there is a continuous change in some aspects of the structure of the membranes as the number of water molecules hydrating the head groups increases from 2 to 16. For the lowest water content, the $W(CO)_6$ environment is very similar to an alkane. As the number of waters of hydration increases, some of the $W(CO)_6$ have increased exposure to the ester portions of DLPC. However, the 2D IR experiments show that there is essentially no change in the dynamics in the interior alkane regions away from the ester-zwitterion head groups. FT-IR studies as a function of cholesterol concentration demonstrate that there is a change in the membrane structure at ∼35% cholesterol. The 2D IR experiments see a sudden change in dynamics at 35% cholesterol. The dynamics are independent of cholesterol content from 10 to 30%. At 35%, the dynamics become slower, and remain unchanged with the slower dynamics constant from 35 to 60% cholesterol.

II. EXPERIMENTAL PROCEDURES

A. Multibilayer Preparation. The experiments are conducted on model membranes composed of aligned multibilayers of DLPC phospholipids.[62,67−70] A multibilayer is like an ordered phase of a liquid crystal. Each bilayer is planar and separated by a water layer. Cells are large with typical sizes of 10 to 30 μm for eukaryotic animal cells. Prokaryotic cells are smaller, typically 1 to 10 μm. Except for the smallest prokaryotic cells, a cell membrane has a large radius of curvature, and over a local region that is small compared to the cell size, it is almost planar. Liposomes and bicelles are much smaller and have much smaller radii of curvatures. Aligned multibilayers eliminate light scattering from liposomes as well as excess water, which absorbs throughout the IR and can interfere with 2D IR experiments. The samples have several thousand individual bilayers. The total sample path is 75 μm. Properly aligned bilayers provide an optically transparent medium.

The DLPC phospholipid and the $W(CO)_6$ vibrational probe were dissolved in dichloromethane and mixed. The solvent was evaporated. For samples with cholesterol, it was also added to the solvent in the appropriate percentage prior to solvent evaporation. The cholesterol concentrations are given as the mole fraction; the sample with 10% cholesterol means there is 1 cholesterol molecule for 9 DLPC molecules. Once the solvent was evaporated, the appropriate quantity of water was added. The amount of water in the sample was verified using Karl Fischer titration.

A small amount of the phospholipid sample was placed between two CaF_2 windows with a Teflon spacer that determines the thickness. A heater, temperature probe, and feedback temperature controller

were used to set the sample temperature for alignment and for the experiments. DLPC was aligned at 50−55 °C, and all of the experiments discussed below were conducted at 45 °C. The windows with the sample were held by a copper sample cell. The bottom of the cell was clapped to the stage of a conoscopic microscope. The top plate of the cell was very slightly loose, and the plate and top window were gently slid around to produce shear that aligned the lipids into a multibilayer. The sample alignment was monitored with the microscope through crossed polarizers. The aligned regions do not rotate the light polarization and appear black. While there are bubbles and regions of unaligned lipid, large regions become aligned. It is only necessary to have aligned spots that are larger than ∼300 μm to completely pass the IR laser beams. Typically there were aligned regions of at least 1 mm and usually several millimeters.

The uniformity of the aligned regions was tested. A small pinhole was placed in the sample cell above the lipid region. The sample cell was mounted on xy translation stages and placed in an FT-IR. The HeNe beam in the FT-IR was put through the pinhole, and the micrometers on the xy stages were read. The micrometers were adjusted to an aligned clear region in the sample, the coordinates were noted, and an FT-IR spectrum was taken. The micrometers were adjusted to other spots and read, and spectra were recorded. The FT-IR spectra demonstrated that most of the aligned samples were uniform from spot to spot. In addition, the measurements were repeated after hours and days, and no changes were found, showing that water did not evaporate from the sealed sample cell.

Following the FT-IR measurements, the sample cell on the xy stages was put into the 2D IR instrument. The IR beams that went into the sample have collinear HeNe alignments beams. The HeNe beams were put through the pinhole, and the xy translation stage coordinates were read. The micrometers were adjusted to the positions on which the FT-IR measurements were made within a few micrometers. Therefore, the 2D IR experiments were performed on the same spots on which the FT-IR spectra were taken.

$W(CO)_6$ is substantially smaller than DLPC. It has a molecular volume of ∼115 Å^3, compared to the ∼675 Å^3 molecular volume of DLPC. In addition, its concentration in the bilayers is small, with 1 $W(CO)_6$ per 800 DLPC molecules in the experiments presented below. Measurements were also made with 1 $W(CO)_6$ per 400 DLPC and 1 $W(CO)_6$ per 200 DLPC. For all of these concentrations, the results were the same. Because the data were very good at the lowest concentration, 1:800, this concentration was used for all of the experiments presented below. Therefore, the presence of $W(CO)_6$ should not have a significant influence on the global structure of the phospholipid bilayers.

B. 2D IR Experiments. A Ti:Sapphire oscillator/regenerative amplifier with repetition rate of 1 kHz, which produced 100 fs pulses with pulse energies of ∼700 μJ and wavelength centered at 800 nm were used to pump a mid-IR optical parametric amplifier (OPA) to generate an ∼170 fs pulse centered at 1980 cm^{-1} with ∼8 μJ pulse energy. The mid-infrared pulse was split into a weaker probe pulse and a stronger pulse. The weak pulse is routed through a mechanical delay line, which is used to set the waiting time T_w (see below). The strong pulse was sent to a mid-infrared Fourier-domain pulse-shaper. Details of the laser system and the pulse shaper have been presented.[35] The output from the pulse shaper, which produces pulses 1 and 2 in the vibrational echo pulse sequence (∼250 μm spot size), was crossed in the sample with the weak probe pulse (pulse 3, 180 μm spot size). The probe is collimated after the sample then sent into a spectrometer acting as a spectrograph equipped with a 32 element HgCdTe infrared array detector.

In a 2D IR vibration echo experiment, τ (the time between pulses 1 and 2) is scanned for a fixed T_w (delay between pulse 2 and 3), which produces a temporal interferogram at each wavelength measured by the spectrograph. Fourier transforming the interferograms gives the horizontal axis (ω_τ axis) and spectrograph gives the vertical axis (ω_m axis) of the 2D spectrum. Then T_w is changed, and τ is scanned to obtain another 2D spectrum. A series of such spectra was recorded for various T_w. The desired information is contained in the T_w dependence of shapes of the peaks in the 2D spectrum (spectral diffusion).

In the pump−probe experiments, two pulses, a strong pump and a weak probe, impinged on the sample. The time between the two pulses is t. The pump produces a transient change in the transmission of the probe. The probe was frequency resolved by the spectrograph, and its amplitude at each frequency was measured as a function of t. The change in probe transmission was obtained with the pump polarization parallel to the probe and at the magic angle of 54.7°.

The frequency−frequency correlation function (FFCF), which quantifies the spectral diffusion in terms of the amplitudes and time scales of the dynamics, is the joint probability that a vibration with an initial (t = 0) frequency in the inhomogeneous spectral distribution will maintain its frequency at a later time t, averaged over all initial frequencies. To extract the FFCF from the 2D spectra, center line slope (CLS) analysis was employed.[71,72] The CLS provides a robust method for determining the FFCF from the 2D IR data that eliminates many systematic errors.[71,72] In addition, it is a direct observable that can be plotted to illustrate the nature of the time dependent spectral diffusion dynamics.

The FFCF was described with a multiexponential model,

$$C_1(t) = \langle \delta\omega_{1,0}(\tau_1)\delta\omega_{1,0}(0)\rangle = \sum_i \Delta_i^2 \exp(-t/\tau_i) \tag{1}$$

where the Δ_i are the frequency fluctuation amplitudes of each component, and the τ_i are their associated time constants. A component of the FFCF with $\Delta\tau < 1$ is motionally narrowed, and it is the dominant source of the homogeneous broadening of the absorption line. When a component is motionally narrowed, Δ and τ cannot be determined separately. The motionally narrowed homogeneous contribution to the absorption spectrum has a pure dephasing line width given by $\Gamma^* = \Delta^2\tau = 1/\pi T_2^*$, where T_2^* is the pure dephasing time. The observed homogeneous dephasing time, T_2, also has contributions from the vibrational lifetime and orientational relaxation:

$$\frac{1}{T_2} = \frac{1}{T_2^*} + \frac{1}{2T_1} + \frac{1}{3T_{or}} \tag{2}$$

where T_2^*, T_1, and T_{or} are the pure dephasing time, vibrational lifetime, and orientational relaxation times, respectively. The total homogeneous line width is $\Gamma = 1/\pi T_2$.

The polarization selective pump−probe technique tracks the decay of the probe transmission with polarizations parallel ($I_\parallel$) and at the magic angle (ma, 54.7°) relative to the pump pulse polarization. The data contain information about both population and orientational dynamics.

$$I_\parallel = P(t)(1 + 0.8C_2(t)) \tag{3}$$

$$I_{ma} = P(t) \tag{4}$$

$P(t)$ is the vibrational population relaxation and $C_2(t)$ is the second Legendre polynomial, which is the transition dipole orientational correlation function for the vibrational mode. Measurements of I_{ma} enable $C_2(t)$ to be extracted from measurements of $I_\parallel$. Here $C_2(t)$ is a single exponential decay characterized by the anisotropy decay time, T_{or}.

The lifetimes of the CO stretch of $W(CO)_6$ in the various samples studied here all are in the range of 110 to 150 ps. Therefore, the lifetime contribution to the homogeneous line width, Γ, is between 0.03 and 0.04 cm^{-1}. The homogeneous line widths measured with the 2D IR experiments discussed below are all ∼3 cm^{-1}. Therefore the lifetime contribution to the homogeneous line width is negligible. The orientational relaxation times, T_{or}, are all ∼6 ps. The orientational relaxation contributes ∼0.6 cm^{-1} to the homogeneous line width. While not negligible, this is a small contribution that does not vary systematically with sample. The homogeneous line widths reported below contain all contributions, but are dominated by the pure dephasing.

The anisotropy decay of the antisymmetric CO stretch of $W(CO)_6$ is not caused by normal molecular reorientation. The CO stretch is

triply degenerate. The excitation pulse projects out a superposition of the three modes that results in the initially excited transition dipole being along the pump pulse electric field.[73] Then fluctuations that cause this initial superposition to change produce a change in the direction of the transition dipole without physical reorientation of the molecule.[73] Therefore, the anisotropy decays in these systems do not provide the type of information that normal orientational relaxation measurements do and cannot be interpreted in terms of shape factors, hydrodynamic boundary conditions, or friction coefficients. Therefore, the orientational relaxation will not be considered further.

III. RESULTS AND DISCUSSION

A. Linear Absorption Spectra of the $W(CO)_6$ Stretching Mode. Figure 1 shows the chemical structure of DLPC.

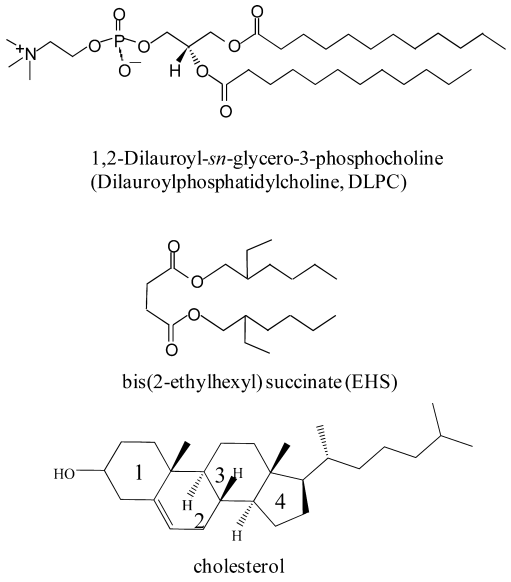

Figure 1. The chemical structures of DLPC (1,2-dilauroyl-*sn*-glycero-3-phosphocholine, dilauroylphosphatidylcholine), top; EHS (bis(2-ethylhexyl) succinate), middle; and cholesterol, bottom.

DLPC can be roughly divided into three regions, the zwitterionic headgroup, the diester moiety, and the alkane chains. Also shown in Figure 1 is the molecule bis(2-ethylhexyl) succinate (EHS). EHS also has a diester region and two hydrocarbon chains. It is a normal organic liquid, and it is used as a model for the nonzwitterionic portions of DLPC. Hexadecane ($C_{16}H_{34}$) is used as a model for the strictly alkane portions of DLPC. In addition, Figure 1 shows the structure of cholesterol, which is added to the model membranes to study its affects on structure and dynamics.

Figure 2A displays the water background subtracted FT-IR spectra of the antisymmetric CO stretch of $W(CO)_6$ in aligned DLPC bilayers as a function of the number of water molecules per DLPC molecule as given in the figure. Note that there is a shoulder on the high frequency side of the spectra at ~1988 cm^{-1} in this FT-IR spectrum and all others discussed below. This shoulder is caused by imperfect background subtraction. The peak is observed in a bilayer sample without $W(CO)_6$. The main source of the absorptive background is water. Making a bilayer sample takes approximately 24 h, and they are not perfectly reproducible. Therefore, a water sample scaled to the water region of the bilayer spectrum was used for the background subtraction. In fitting the spectra, this shoulder was not included.

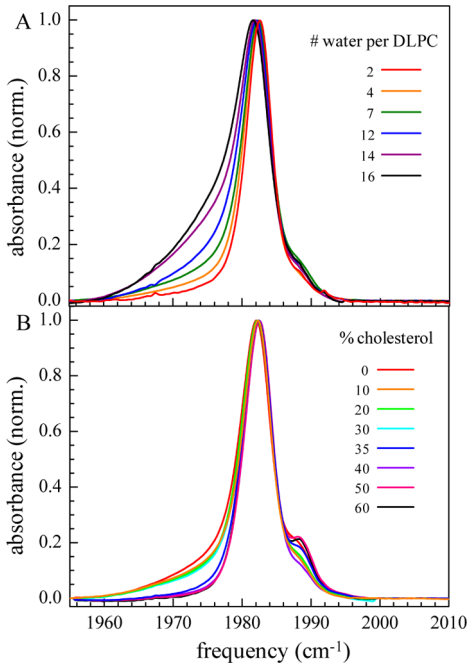

Figure 2. (A) Water background subtracted FT-IR absorption spectra of the CO antisymmetric stretching mode of $W(CO)_6$ in aligned DLPC bilayers with various numbers of water, 2, 4, 7, 12, 14, and 16, per headgroup. As the number of waters of hydration increases, a wing on the low frequency side of the absorption line becomes larger. (B) Background subtracted FT-IR absorption spectra of the CO antisymmetric stretching mode of $W(CO)_6$ in aligned DLPC bilayers with 8 waters of hydration for various concentrations of cholesterol, 0–60%. As the concentration of cholesterol increases, the wing on the low frequency side of the absorption decreases. There is a sudden decrease in the size of the wing going from 30 to 35% cholesterol.

The most prominent feature associated with increasing the number of hydrating water molecules from 2 to 16 is the continuous growth of a wing on the low frequency side of the line. The FT-IR spectrum of $W(CO)_6$ in DLPC multibilayers with 25 waters of hydration (not shown) is identical to the spectrum with 16 waters of hydration. Thus, the bilayers with 16 waters of hydration are fully hydrated. The bilayer spectra with the various numbers of hydrating water molecules are discussed in detail below.

Figure 2B displays the CO stretch absorption as a function of cholesterol concentration. All samples have 8 water molecules per DLPC. The change in the spectra with cholesterol concentration is bimodal in regard to the low frequency wing. In going from 0 to 10% cholesterol, the wing becomes only slightly smaller. However, the 10, 20, and 30% spectra are almost identical. Then in going from 30 to 35% there is a jump; the wing is basically gone. The 35% sample spectrum is almost the same as the higher concentration samples, with the 40, 50, and 60% spectra being essentially identical. So the spectra divide into two groups, those with less than 35% cholesterol, and those with 35% or more cholesterol, as discussed in detail below.

Figure 3 displays the CO stretch spectra of $W(CO)_6$ in two liquids, EHS and hexadecane. As can be seen in Figure 3, $W(CO)_6$ in hexadecane has an exceedingly narrow line width compared to the width in EHS (15.2 cm^{-1}). The line width in EHS is more typical. For example, the CO antisymmetric stretch of $W(CO)_6$ in CCl_4 and in $CHCl_3$ are 10 cm^{-1} and 19

dx.doi.org/10.1021/ja403675x | J. Am. Chem. Soc. 2013, 135, 11063–11074

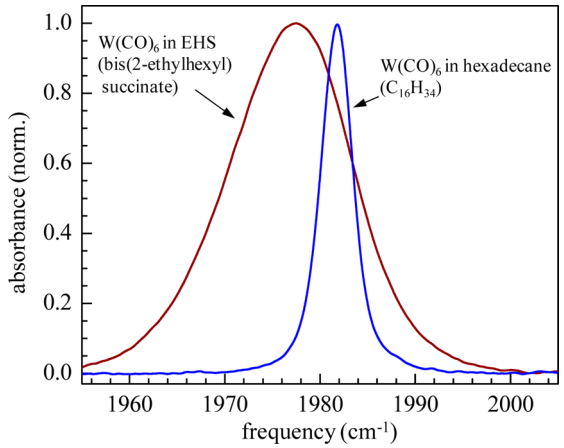

Figure 3. Background subtracted FT-IR absorption spectra of the CO antisymmetric stretching mode of $W(CO)_6$ in EHS (bis(2-ethylhexyl) succinate) and in hexadecane. These spectra are used to model the spectra in DLPC.

cm^{-1}, respectively.[74] Long linear hydrocarbons like hexadecane tend to have all trans configurations, which will produce little variation in the environment experienced by $W(CO)_6$, yielding the narrow line width. In EHS, $W(CO)_6$ can experience a wider range of environments giving rise to a broader line. In EHS, $W(CO)_6$ can be in an alkane environment or it can interact with the ester moieties (see Figure 1). Given the spectrum in hexadecane, presumably the high frequency side of the EHS line corresponds to more alkane-like environments. The $W(CO)_6$ does not have to come in direct contact with an ester oxygen to have its frequency shifted. As has been shown by comparison between experiments and simulations, frequency shifts that give rise to inhomogeneous broadening of vibrational absorption lines can arise from variations in the local electric field. Such variations can be caused by proximity to the ester moieties of EHS.[75−77]

1. Effects of Waters of Hydration. Figure 4 shows a comparison of the CO stretch spectra of $W(CO)_6$ in aligned DLPC bilayers with 2 water molecules per headgroup (DLPC/2water) and hexadecane. While not identical, the two spectra

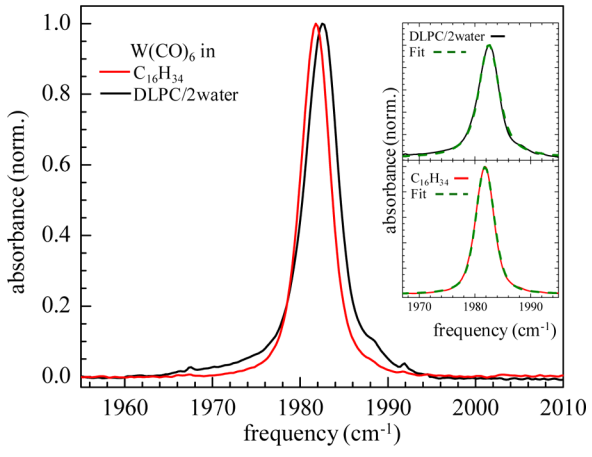

Figure 4. Background subtracted FT-IR absorption spectra of the CO antisymmetric stretching mode of $W(CO)_6$ in DLPC with 2 waters of hydration and in hexadecane ($C_{16}H_{34}$). The spectra are very similar. The insets show Voigt line shape fits to the spectra. Both are symmetrical and well fit as Voigt line shapes.

are very similar. The insets in Figure 4 show Voigt fits to the two absorption bands. The spectrum in DLPC/2water is centered at 1982.4 ± 0.1 cm^{-1} and has a full width at half-maximum (fwhm) of 4.35 ± 0.03 cm^{-1}. The spectrum in hexadecane is centered at 1981.8 ± 0.1 cm^{-1} and has a fwhm of 3.7 ± 0.01 cm^{-1}. These results indicate that at the very low water hydration level of 2 waters per DLPC, the $W(CO)_6$ experiences an alkane environment.

As shown in Figure 2A, an increasingly large wing on the low frequency side of the spectrum grows in as the number of water molecules per DLPC is increased. To model the changes in the spectrum with increasing water content, we employ the $W(CO)_6$ in EHS spectrum (see Figure 3). The $W(CO)_6$ in EHS spectrum was fit with a Voigt line shape, although it is almost Gaussian. The $W(CO)_6$ in EHS CO stretch spectrum is centered at 1976.8 ± 0.1 cm^{-1} with a fwhm of 15.2 ± 0.2 cm^{-1}. We fit all of the other spectra in Figure 2A as the sum of the DLPC/2water spectrum and the EHS spectrum, with their relative amplitudes allowed to vary. In all of the fits, the EHS parameters, center frequency, width, and shape were fixed. For the DLPC/2water spectrum, the width and shape were fixed. However, at high water content the DLPC/2water spectrum was shifted somewhat to lower frequency to improve the fits, with 0.8 cm^{-1} the largest shift for 16 waters per DLPC.

Figure 5 shows the results of the fits of the experimental CO stretch spectra to the sum of the $W(CO)_6$ in EHS and DLPC/2water spectra. The top panel is the spectrum in DLPC with 16 waters per headgroup (DLPC/16water). This is the spectrum with the largest wing. As can be seen in the figure, the fit is excellent. The middle panel shows the fit to the DLPC/7water spectrum, and the bottom panel shows the fit to DLPC/4water spectrum. In each case, the fits do a very good job of reproducing the data. The fits to the other spectra shown in Figure 2A are equally good. These results show that with more water the larger wing arises from greater interaction of $W(CO)_6$ with the ester part of DLPC.

As shown in Figure 4, the FT-IR spectrum of $W(CO)_6$ in DLPC/2water is a symmetric Lorentzian with no red side wing. This spectrum reflects $W(CO)_6$ in a pure alkane environment. From the fits, the ratios of the areas (A) of the $W(CO)_6$ in DLPC/2water spectrum to the $W(CO)_6$ in EHS spectrum ($A_{DLPC/2water}/A_{EHS}$) for DLPC/4water, DLPC/7water, DLPC/12water, DLPC/14water, and DLPC/16water are 6.0, 3.0, 2.1, 1.1, and 0.9, respectively. The results of the fits in Figures 4 and 5 show that the $W(CO)_6$ experiences both alkane and ester environments but with the interaction with the ester region of DLPC bilayers increasing as the number of waters of hydration increases. Even for DLPC/16water, the dominant interaction is with the alkane portion of the bilayer, as one of the components in the fit is essentially pure alkane (see Figure 4) and the other component of the fit uses the molecular solvent EHS, which is predominately alkane but also part ester.

The spectroscopic trends with increasing water of hydration (Figures 2A and 5) can be considered in the light of X-ray structure, EPR, and neutron diffraction experiments, as well as molecular dynamics simulations on lipid bilayers as a function of the number of the hydration level.[78−83] These studies show that upon hydration, the structure of the bilayers change. The thickness of the membrane decreases, while the area per lipid increases. This increase in area with increased water causes the side chains to tilt relative to the bilayer plane. Thus, the changes in the $W(CO)_6$ spectrum appear to be reporting on the structural changes induced by increased number of waters of

dx.doi.org/10.1021/ja403675x | J. Am. Chem. Soc. 2013, 135, 11063−11074

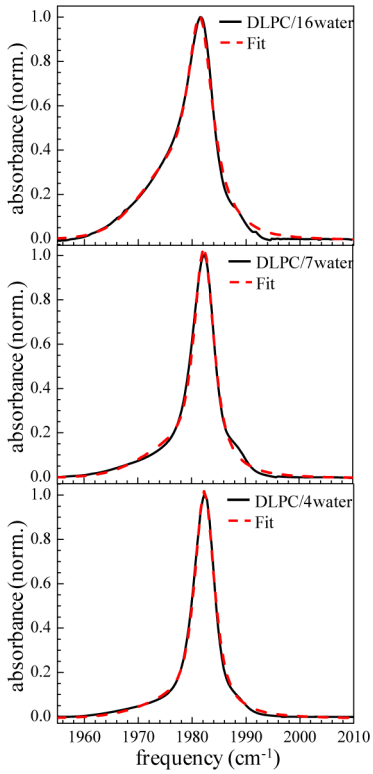

Figure 5. Background subtracted FT-IR absorption spectra of the CO antisymmetric stretching mode of $W(CO)_6$ in DLPC with 16 (top), 7 (middle), and 4 (bottom) waters of hydration (solid black curves) and fits to the data (dashed red curves). The fits are the sum of two Voigt line shapes, one with the EHS parameters (see Figure 3) and one with the DLPC with 2 waters of hydration parameters (see Figure 4). The wings on the low frequency side of the spectra are reproduced by varying amplitudes of the $W(CO)_6$ CO stretch in EHS spectrum. The amplitude decreases as the number of waters of hydration decreases showing less interaction with the ester moiety of DLPC. See text.

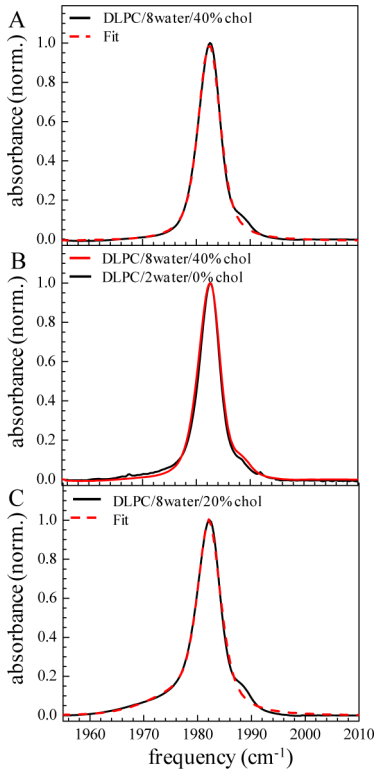

Figure 6. (A) Background subtracted FT-IR absorption spectra of the CO antisymmetric stretching mode of $W(CO)_6$ in aligned DLPC bilayers with 8 waters of hydration and 40% cholesterol (black curve) and a fit to a Voigt line shape function (dashed red curve). The line shape is a symmetric Voigt. (B) A comparison between the spectra $W(CO)_6$ in DLPC with 8 waters of hydration and 40% cholesterol (red curve) and DLPC with 2 waters of hydration and 0% cholesterol (black curve). The two spectra are virtually identical. (C) The FT-IR spectrum of $W(CO)_6$ in aligned DLPC bilayers with 8 waters of hydration and 20% cholesterol (solid black curve) and a fit to the data (dashed red curve). The fit is the sum of two Voigt line shapes, one with the EHS parameters (see Figure 3) and one with the DLPC with 8 waters of hydration and 40% cholesterol parameters (see panel A). The wing on the low frequency side of the spectrum is reproduced by the contribution of the $W(CO)_6$ CO stretch in EHS spectrum. See text.

hydration and result in the increased interaction of the $W(CO)_6$ with the ester portion of DLPC. The influence of the level of hydration on the bilayer structural dynamics is discussed below in Section III.B.1.

2. Effects of Cholesterol. Returning to Figure 2B, it can be seen that the effect of cholesterol on the $W(CO)_6$ CO stretch spectrum in DLPC/8water is fundamentally different from the influence of the number of waters of hydration. The spectra with 10, 20, and 30% cholesterol are essentially identical and are only slightly different from the spectrum with no cholesterol. At 35% cholesterol, the spectrum changes; the wing on the low frequency side of the line vanishes. The 35% spectrum is almost the same as the 40, 50, and 60% spectra, which are identical.

The Figure 6A shows one of the identical spectra, the spectrum with 40% cholesterol and a fit to a Voigt function; the line is symmetrical and well described as a Voigt profile. (Recall that the small shoulder at ~1988 cm^{-1} is caused by imperfect background subtraction.) The symmetric shape is in contrast to the spectrum in DLPC/8water with no cholesterol that has a pronounced wing on the low frequency side of the line (red curve in Figure 2B). Figure 6B shows a comparison of the spectrum in DLPC/8water/40% cholesterol and the spectrum in DLPC/2water with no cholesterol. These two spectra are almost identical. (The Voigt fit to the DLPC/2water/0% cholesterol is shown in the inset of Figure 4.)

Figure 6C shows the spectrum for DLPC/8water/20% cholesterol and a fit performed in a manner similar to that used to fit the spectra at different levels of hydration (see Figure 5). The spectrum in DLPC/8water/20% cholesterol was fit using the sum of the spectra from DLPC/8water/40% cholesterol (see Figure 6A) and EHS (see Figure 3). The fit is very good. So at low cholesterol concentration, ≲30%, the $W(CO)_6$ interacts with the ester portions of DLPC to some extent. The ratio of the areas of the fit, $A_{20\%}/A_{EHS}$ = 3.6. Thus, the dominant interactions are with the alkane portions of DLPC, but there is some exposure to the esters. However, at high cholesterol concentration, ≳35%, the spectra are symmetric and virtually the same as the spectrum from the DLPC/2water and hexadecane (see Figure 4). Therefore, for ≳35% cholesterol, the interactions are exclusively with the alkane chains. The spectra show that there is an abrupt change between 30 and 35% cholesterol. These results demonstrate spectroscopically that there is a sudden change in the interior bilayer structure between 30 and 35% cholesterol. This change is also observed

dx.doi.org/10.1021/ja403675x | J. Am. Chem. Soc. 2013, 135, 11063−11074

in the dynamical measurements presented below in Section III.B.2.

An interesting general aspect of the FT-IR results presented above is that the CO antisymmetric stretching mode of $W(CO)_6$ is sensitive to the internal structure of the bilayers. FT-IR studies are relatively simple experiments. It is possible that $W(CO)_6$ can be used to study structural changes in bilayers induced by wide variety of influences. It is possible that $W(CO)_6$ can be placed in the membranes of living cells and used as a probe for changes in structure as well as dynamics. Metal carbonyls have been inserted into live cell membranes for Raman and SERS imaging.[84,85]

B. Dynamical Measurements. Figure 7 displays 2D IR vibrational echo spectra taken on the antisymmetric CO stretch

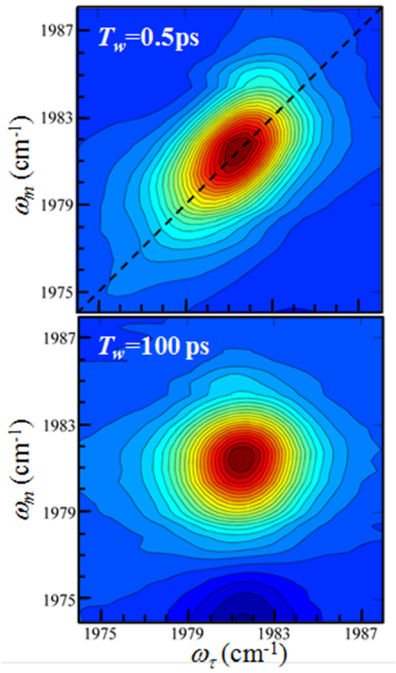

Figure 7. 2D IR vibrational echo spectra of the CO antisymmetric stretching mode of $W(CO)_6$ in aligned DLPC bilayers with 16 waters of hydration. Top panel, short T_w = 0.5 ps. Bottom panel, long T_w = 100 ps. The top panel shows the diagonal, dashed line.

of $W(CO)_6$ in aligned DLPC bilayers with 16 waters of hydration. The panels show the portions of the 2D spectra that correspond to the 0−1 vibrational transition. The top spectrum is taken at a short T_w = 0.5 ps. The bottom spectrum is taken at a relatively long T_w = 100 ps. The dashed line in the top spectrum is the diagonal. At short time, the 2D IR spectrum is substantially elongated along the diagonal. However, by 100 ps, the shape has changed substantially, and the spectrum is almost symmetrical about the diagonal. The change in shape with increasing T_w provides the information on spectral diffusion and, therefore, the time dependence of the structural evolution of the system.

While the FT-IR spectrum for DPLC with more than 2 waters of hydration show asymmetrical line shapes that were resolved into $W(CO)_6$ in an alkane-like portion and $W(CO)_6$ in a portion modeled with EHS, which is composed of both alkane and ester moieties (see Figures 2A and 5). For the lower water concentrations (<∼14 waters of hydration), the non-alkane contribution to the spectrum is small and results in negligible contribution to the 2D IR spectrum that is analyzed with the CLS method in the wavelength range (∼1980 to ∼1984 cm^{-1}) corresponding to the alkane region (see Figure 4). For the higher water concentrations, particularly 16 waters of hydration, the EHS-like shoulder has significant area. However, the fraction of the EHS shoulder that falls within the range used in the CLS analysis is small, and part of it is alkane-like. In addition to its broad width reducing the amplitude of the 2D IR spectrum at a given wavelength, qualitative analysis shows that the CO stretch of $W(CO)_6$ in the ester region of the bilayer has a substantially larger homogeneous component. Looking at the smallest contours at short time, it is possible to see the 2D IR spectrum well to the red (<1970 cm^{-1}) of the spectrum shown in Figure 7. The amplitude of the data is not sufficient for quantitative analysis, but it is possible to see that the spectrum is very broad in the antidiagonal direction (perpendicular to the dashed line in the upper panel of Figure 7). This large width is caused by substantial homogeneous broadening, which further reduces the amplitude of the signal by spreading it out in the antidiagonal direction. The large homogeneous width of the CO stretch of $W(CO)_6$ in the ester region may be caused by very fast structural fluctuations of the nearby water molecules.

The net result is that even for 16 waters of hydration, the data analysis for all of the 2D IR data are from $W(CO)_6$ in the alkane interior of the bilayer with essentially no contribution from $W(CO)_6$ in the ester regions. It should be possible using different vibrational probes to study the ester and headgroup regions of the bilayers.

As mentioned in Section II.B, the change in shape of the 2D IR spectra with increasing T_w is quantified using the CLS method.[71,72] The CLS analysis provides a mechanism for obtaining the FFCF from the 2D IR data. The CLS varies from 1 at T_w = 0 to 0 at sufficiently long time such that all frequencies in the inhomogeneously broadened absorption line have been sampled, that is, when all structures that contribute to the inhomogeneous line have been sampled. The CLS will only be 1 at T_w = 0 if there is no homogeneous component to the absorption line. The homogeneous component is manifested as the difference from 1 of the T_w = 0 value of the measured CLS. Using the CLS method, this difference from 1 gives the homogeneous component of the FFCF.

1. Effects of Waters of Hydration. First we consider the influence of increasing the numbers of waters of hydration of the DLPC head groups on the interior structural dynamics of the membranes observed from the perspective of the interior alkane region of the bilayers. The samples studied contained 2, 4, 7, 8, 12, 14, and 16 waters per headgroup. Figure 8A shows CLS decay curves for three of these, 2, 8, and 16. The points are the data, and the solid curves are the biexponential fits. As can be seen in the figure, these curves, and in fact all of the curves for the other numbers of waters, are virtually identical. The curves are fit very well with biexponential decay functions. Figure 8B shows a plot of the slow and fast components for each sample. In spite of the fact that the curves appear almost identical to the eye, fitting with a biexponential function produces some variation in the time constants. The error bars are the errors in the biexponential fits. However, there can be additional systematic errors that can cause the data points to vary somewhat outside of the fit error bars. The horizontal lines are the average values of the time constants obtained from the fits. From Figure 8A,B it is clear that increasing the headgroup hydration does not impact the internal structural dynamics of the membrane's interior alkane regions. While there is some

dx.doi.org/10.1021/ja403675x | J. Am. Chem. Soc. 2013, 135, 11063−11074

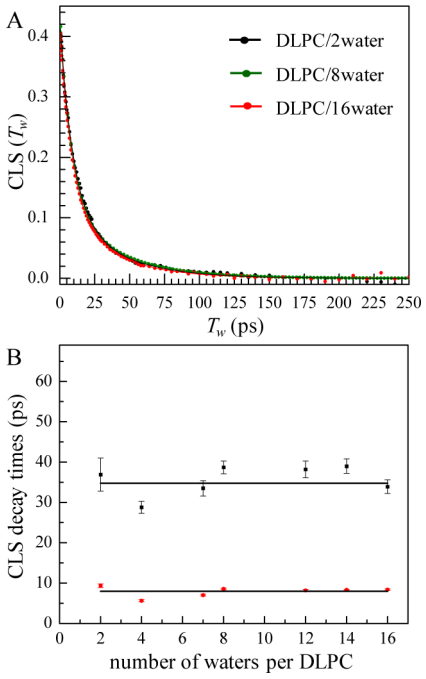

Figure 8. (A) Center line slope (CLS) decay curves obtained from the 2D IR spectra of the CO antisymmetric stretching mode of $W(CO)_6$ in DLPC with 16 (red), 8 (green), and 2 (black) waters of hydration. The decay curves are essentially identical, showing that there is no dependence on the internal bilayer dynamics on the number of waters of hydration. (B) Fast and slow decay time constants obtained from a biexponential fits to the CLS decay curves for the various number of waters of hydration. Although there is scatter in the fit values, there is no systematic change in the parameters with the number of waters of hydration, showing that there is no dependence of the interior bilayer dynamics on the number of waters of hydration.

scatter in the data, both the fast and slow components do not systematically vary with the number of waters of hydration.

The FFCF (see eqs 1 and 2) and the vibrational lifetime parameters are given in Table 1. Because all of the curves were so similar (see Figure 8A), the values in Table 1 are the average of the fits to all of the experimental curves for the various number of waters per headgroup. The individual time constants are displayed in Figure 8B. The lifetime value, T_1 = 110 ps, given in Table 1 is for the CO stretch of $W(CO)_6$ in the alkane interior of the bilayers. By performing the pump−probe experiment in the low frequency portion of the spectrum, we were able to obtain a value for the lifetime for the CO stretch of $W(CO)_6$ in the ester region of the bilayer, i.e., $T_1 = 37 \pm 6$ ps. The large difference in the lifetimes in the two regions confirms that the $W(CO)_6$ is located in very different environments. The fact that two distinct lifetimes are observed shows that $W(CO)_6$ does not move on a picosecond time scale between the two regions.

It is worth noting that a 2D IR study of AOT (sodium bis(2-ethylhexyl) sulfosuccinate) bilayers also using the CO stretch of $W(CO)_6$ as the probe showed that there is no change in the internal bilayer dynamics as a function of the number of waters hydrating the sulfonate head groups.[86] The structural fluctuations in the AOT lamellae were slower, with the fast and slow components of the dynamics being ∼12.5 and ∼150 ps, respectively. The fast component in AOT is somewhat slower, while the slow component is approximately a factor of 4 slower. While the dynamics inside the AOT lamellae did not show a change with the number of waters of hydration, they did change with a phase transition from lamellar to bicontinuous cubic structure.[86]

Figure 2A shows that there is a continuous change in the CO stretch absorption spectrum with the number of waters of hydration, while Figure 8A,B shows that there is no change in the internal structural dynamics observed in the alkane regions of the bilayers within experimental error. The 2D IR time dependent spectra measure the evolution of the molecular vibrational frequency caused by structural changes. The analysis of the spectra in Figure 2A shows that as the number of waters of hydration increases, an increasing fraction of $W(CO)_6$ is exposed to the ester portion of DLPC. The absorption spectrum is highly sensitive to very local intermolecular interactions. The spectra as well as many other studies[78−82] show that changing the number of waters of hydration changes the bilayer structure. However, the results in Figure 8A,B demonstrate that changes in the headgroup structure of the bilayers does not change the dynamics in the alkane interior of the bilayers. The water content results are not caused by a lack of sensitivity to changes in the dynamics, as demonstrated below in the analysis of the influence of cholesterol on membrane dynamics. Simulations of DLPC bilayer interior ultrafast structural fluctuations would help clarify the physical reasons for the observed water independent dynamics.

2. Effects of Cholesterol. The investigation of the affects of cholesterol on the membrane bilayers uses samples with a fixed number of waters of hydration, 8 per DLPC. Eight water molecules are sufficient to hydrate the head groups,[87] and in the absence of cholesterol there is no difference in the alkane interior dynamics with the number of waters of hydration. As discussed above in connection to Figures 2B and 6, addition of cholesterol causes a discontinuous change in the spectrum. The abrupt change in the FT-IR spectra between 30 and 35% cholesterol is a sign of a sudden change in the internal membrane structure. Figure 9A displays CLS decay curves for two cholesterol concentrations, 20 and 40%, which are on either side of the 30−35% break in the spectral line shapes. The points are the data, and the solid curves are the fits. Both curves are well fit with biexponential functions. The results show that the decay constants are significantly different. This is in contrast to the CLS curves displayed in Figure 8A, where changing the number of waters of hydration did not change the decay curves.

Table 1. FFCF (see eqs 1 and 2) and Vibrational Lifetime (T_1) Parameters for DLPC/Water with 0% Cholesterol[a]

Γ (cm^{-1})	T_2 (ps)	Δ_1 (cm^{-1})	τ_1 (ps)	Δ_2 (cm^{-1})	τ_2 (ps)	T_1 (ps)
2.9 ± 0.3	3.6 ± 0.4	1.2 ± 0.2	7.5 ± 0.8	0.9 ± 0.1	35.4 ± 2	110 ± 3.1

[a]As discussed in the text, the decay curves are virtually identical (see Figure 8A), and therefore, the parameters in the table are the average values of the fits to the data obtained from all of the samples with different numbers of waters of hydration. The Δ's are standard deviations. The total inhomogeneous line width is the convolution of the two Gaussian contributions, i. e., $(\Delta_1^2 + \Delta_2^2)^{1/2}$. The fwhm is obtained by multiplying this number by 2.35. The total line width (fwhm) is the total inhomogeneous fwhm convolved with the homogeneous Lorentzian component fwhm, Γ.

dx.doi.org/10.1021/ja403675x | J. Am. Chem. Soc. 2013, 135, 11063−11074

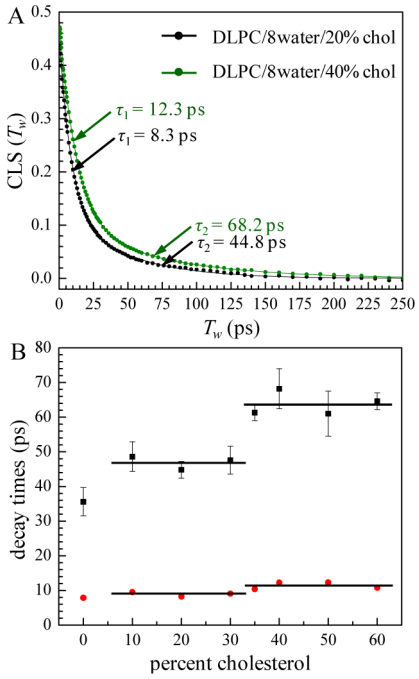

Figure 9. (A) CLS (center line slope) decay curves obtained from the 2D IR spectra of the CO antisymmetric stretching mode of $W(CO)_6$ in DLPC with 8 waters of hydration and with 20% (black curve) and 40% (green curve) cholesterol. The dynamics differ because of the difference in cholesterol concentration. (B) Fast and slow decay time constants obtained from a biexponential fits to the CLS decay curves for the various percent concentrations of cholesterol in DLPC with 8 waters of hydration. There is an abrupt slowing of the dynamics in going from 30 to 35% cholesterol, while samples with 10, 20, and 30% have essentially the same slow and fast values, and samples with 35, 40, 50, and 60% cholesterol have essentially the same slow and fast values. See Table 2 for the values of the time constants. The black lines correspond to the average values.

Figure 9B displays the results of the CLS fits to all of the cholesterol concentration dependent data. The two time constants from the biexponential fits are plotted. The points at 0% are the time constants from the DLPC with 8 waters of hydration sample. The time constants and the rest of the FFCF parameters as well as the vibrational lifetimes, T_1, are given in Table 2. It is clear from Figure 9B that the bilayer alkane interior structural dynamics, as manifested through the spectral diffusion time constants, behave in a manner analogous to the spectra shown in Figure 2B. In going from 0 to 10% cholesterol, there is a slowdown of the dynamics. However, the samples with 10, 20, and 30% cholesterol have identical dynamics within experimental error. Then at 35% cholesterol the dynamics slow substantially, and then the dynamics are constant in the range 35−60% cholesterol. The slowing of the dynamics at high cholesterol concentrations is more evident in the slow component, τ_2, but both components exhibit a sudden change, which is outside of experimental error. In the range 10−30%, the average slow component time constant is 47 ps, while in the 35−60% range, the average slow component time constant is 64 ps. For the fast components, the averages over the same two ranges give 9 and 11.5 ps. The T_2 values (homogeneous dephasing times) in Table 2 also appear to have a break at 35% cholesterol.

The spectra shown in Figure 2B indicate a change in the local environment experienced by $W(CO)_6$ at 35% cholesterol. The vibrational lifetime decay time (T_1) is very sensitive to the local environment of the vibrational probe. The T_1 values listed in Table 2, which are measured at the peak of the spectrum (alkane region) also show a jump between low and high concentration cholesterol. For ≤30% cholesterol, the average T_1 is 121 ps. For >35% cholesterol, the average T_1 is 146 ps. The point right at 35% is ambiguous because of the large error bar. In the spectra shown in Figure 2B, the 35% cholesterol spectrum was almost but not quite the same as spectra for higher concentrations. The lifetime for 35% may also be intermediate between the high and low concentration values.

The structure of cholesterol is shown in Figure 1. Other than the hydroxyl group, the molecule is a hydrocarbon. The hydroxyl can make two hydrogen bonds with water since it is both a hydrogen bond donor and acceptor. Therefore, the hydroxyl locates at or near the surface of the membrane where it can interact with water. X-ray experiments show that the length of the cholesterol molecule is 16 Å.[88] Therefore, leaving out the DLPC zwitterion headgroup and the cholesterol hydroxyl, both of which will be hydrated by water, DLPC and cholesterol are approximately the same length. Cholesterol has 4 rings with a single double bond and a 6 carbon chain in contrast to DLPC in which the hydrocarbon portions are linear alkanes. In the interior of the membrane, $W(CO)_6$ interacting with the DLPC hydrocarbon chains may not be much different in terms of influencing the CO stretch absorption spectrum than interacting with hydrocarbon portion of cholesterol.

DLPC bilayers with 8 waters of hydration and 0% cholesterol has a relatively small but readily observable wing on the low frequency side of the $W(CO)_6$ CO stretch absorption line (see Figure 2B). This wing has been accounted for as arising from a degree of interaction of the $W(CO)_6$ with the DLPC ester

Table 2. FFCF (see eqs 1 and 2) and Vibrational Lifetime (T_1) Parameters for DLPC with 8 Waters Per Head Group and Varying Amounts of Cholesterol[a]

sample	Γ (cm^{-1})	T_2 (ps)	Δ_1 (cm^{-1})	τ_1 (ps)	Δ_2 (cm^{-1})	τ_2 (ps)	T_1 (ps)
10%	3.5 ± 0.3	3.0 ± 0.2	1.3 ± 0.2	9.5 ± 0.3	0.7 ± 0.3	49 ± 4	125 ± 2
20%	3.5 ± 0.1	3.0 ± 0.1	1.4 ± 0.1	8.3 ± 0.2	0.9 ± 0.1	45 ± 2	117 ± 3
30%	3.4 ± 0.2	3.2 ± 0.2	1.3 ± 0.2	9.1 ± 0.3	0.9 ± 0.1	48 ± 4	120 ± 3
35%	3.0 ± 0.3	3.6 ± 0.3	1.4 ± 0.2	10.4 ± 0.1	0.8 ± 0.2	61 ± 2	126 ± 9
40%	2.6 ± 0.2	4.0 ± 0.2	1.3 ± 0.1	12.3 ± 0.2	0.7 ± 0.2	68 ± 6	147 ± 1
50%	2.8 ± 0.3	3.7 ± 0.1	1.4 ± 0.1	12.3 ± 0.3	0.7 ± 0.1	61 ± 6	143 ± 3
60%	2.6 ± 0.1	4.0 ± 0.2	1.4 ± 0.2	10.8 ± 0.1	0.7 ± 0.2	65 ± 2	147 ± 2

[a]The Δ's are standard deviations. The total inhomogeneous line width is the convolution of the two Gaussian contributions, i.e., $(\Delta_1^2 + \Delta_2^2)^{1/2}$. The fwhm is obtained by multiplying this number by 2.35. The total line width (fwhm) is the total inhomogeneous fwhm convolved with the homogeneous Lorentzian component fwhm, Γ.

dx.doi.org/10.1021/ja403675x | J. Am. Chem. Soc. 2013, 135, 11063−11074

moiety (see discussion surrounding Figure 5). However, as discussed in detail above, the 2D IR spectral analysis focuses only on the signal from those $W(CO)_6$ molecules in the interior, alkane regions of the bilayers. Therefore, changes in dynamics measured by the 2D IR experiments are associated with changes in the alkane chain dynamics with essentially no direct contribution from the ester/headgroup regions of the bilayers. In going from 0 to 10% cholesterol, the wing decreases very slightly and then remains essentially constant for 10, 20, and 30% cholesterol. The bilayer internal structural dynamics measured by the spectral diffusion (see Figure 9B and Table 2) become slower in going from 0 to 10% cholesterol and then are constant for 10, 20, and 30% cholesterol. As mentioned earlier, the addition of cholesterol to phospholipid bilayers decreases the area of the headgroup[9] and presumably the volume per phospholipid molecule, and it also decreases the depth of water penetration into the bilayer.[89,90] Such changes can modify the interior alkane chain structure of the membrane and could be responsible for the changes in both the spectrum and the dynamics in going from 0 to the 10−30% cholesterol concentrations. However, the results presented here show that going from 10 to 30% cholesterol in DLPC bilayers with 8 waters of hydration at 45 °C produces no additional changes that are experienced by the $W(CO)_6$ vibrational probe in either the spectrum or the dynamics. These results indicate a change in structure with the first addition of cholesterol (0−10%) but no significant changes from 10 to 30%. It is possible that in the 10−30% cholesterol concentration range, the DLPC bilayers are in the liquid-disorder (L_d) phase with the acyl chains containing gauche bonds, which reorient them away from the bilayer normal. L_d phase has been observed for other phospholipids at low cholesterol concentrations.[23,30,91]

In going from 30 to 35% cholesterol there is a fundamental change in the nature of the system. The wing on the low frequency side of the spectrum vanishes (see Figure 2B) and the dynamics slow (see Figure 9A,B). These sudden changes with a small change in cholesterol concentration suggest a structural phase transition in the interior alkane region of the bilayers, particularly given that both the spectrum and the dynamics do not change further over the range of cholesterol concentrations from 35 to 60%.

The bilayer structure that gives rise to the $W(CO)_6$ alkane environment at high cholesterol concentration may involve less free volume and tighter packing liquid-order (L_o) phase, which results in the slower structural dynamics. In a study using acousto-optical methods it was shown that dipalmitoylphosphatidylcholine (DPPC) undergoes a sharp change in mechanical properties when the cholesterol concentration is increased.[10] DPPC bilayers at ∼45 °C display a break in both the in-plane anisotropic viscosity and the anisotropic bulk modulus at ∼20% cholesterol. The bulk modulus, which is a measure of the resistance to compression, has a sharp increase at 20% cholesterol. The bulk modulus is a macroscopic property. Its sudden increase can be attributed to a decrease in the free volume of the DPPC/cholesterol bilayer internal molecular structure. EPR studies of DPPC show sudden changes in residual homogeneous line widths at 20% cholesterol going from L_d to L_o phase.[30] These types of changes may occur in the DLPC bilayers between 30 and 35% cholesterol. A reduction in free volume of the L_o phase resulting in tighter packing in the bilayer could produce the observed slowing of the molecular level structural dynamics measured with the 2D IR spectral diffusion experiments.

At high cholesterol concentration the $W(CO)_6$ FT-IR spectrum is very similar to that in hexadecane (see Figure 4). The 2D IR measures the dynamics in the interior alkane region of the bilayers. It is informative to compare the dynamics in the bilayers and in hexadecane. The spectral diffusion time constants for the CO antisymmetric stretch of $W(CO)_6$ in hexadecane are τ_1 = 4.9 ps and τ_2 = 19.8 ps. In contrast, at high cholesterol concentrations the corresponding decay times are ∼11.5 ps and ∼64 ps. Although the spectra in hexadecane and high concentration cholesterol/DLPC are virtually the same, the dynamics are substantially slower in the ordered bilayer environment. At low cholesterol concentration, the dynamics in the DLPC bilayers are faster, and with no cholesterol, they are even faster, but all are still slower than in hexadecane (see Tables 1 and 2).

IV. CONCLUDING REMARKS

The results presented above investigate the ultrafast structural dynamics of phospholipid model membranes in their interior alkane regions. The nonpolar and hydrophobic vibrational probe, $W(CO)_6$, placed inside of the bilayers at low concentration, reports on its environment through the CO antisymmetric stretch vibrational absorption spectra and on the internal structural dynamics of the model membranes through the time dependence of the 2D IR vibrational echo spectra. The experiments conducted on aligned DLPC multibilayers examined the influence of the number of waters of hydration of the phospholipid head groups and the concentration of cholesterol on dynamics and structure. The results show that the dynamics in the interior alkane region of the bilayers do not depend on the number of waters of hydration (see Figure 8A,B), although FT-IR absorption measurements demonstrate that there is some degree of structural changes of the bilayers with hydration level (see Figures 2A and 5). In contrast to the lack of changes in alkane interior structural dynamics caused by water on the outside of the membranes, the addition of cholesterol does change the interior structural dynamics of the bilayer. Adding cholesterol slowed the dynamics, but the slower dynamics are independent of cholesterol concentration in the range of 10−30%. However, at 35% cholesterol there is a sudden change, and the dynamics become even slower (see Figure 9A,B). The abrupt change between 30% and 35% cholesterol is also evident in the FT-IR spectra (see Figure 2B) and may be caused by a phase change.

A large number of biological processes occur in phospholipid membranes and membranes composed of other types of lipids. The portion of a transmembrane protein that is embedded in a membrane has dynamical interactions with its membrane environment. The dynamics of internal protein processes are coupled to the membrane medium. The selectivity of transmembrane proteins to pass particular ions and neutral species in and out of a cell depends on specific chemical interactions along the transport pathway. However, the movement from point to point on the pathway requires protein structural fluctuations that are coupled to the structural fluctuations of the membrane. Knowledge of the structural dynamics of membranes and how the dynamics are changed by other molecular species such as cholesterol, transmembrane peptides, or proteins can inform our understanding of membrane biological processes.

The work presented above brings up a large number of questions that can be answered using the methods employed here. How different are the dynamics of DLPC and DPPC; that

is, what is the side chain length dependence? Does cholesterol affect DLPC and DPPC in the same manner? How do the ultrafast dynamics in vesicle bilayers differ from the planar bilayers studied here, and how do possible differences depend on the radius of curvature (size) of the vesicles? DLPC has saturated hydrocarbon side chains. How does the inclusion of lipids with double bonds influence the ultrafast dynamics, and what is the concentration dependence of the influence? These are a few of the many interesting issues that can be addressed. Finally, these experiments are excellent targets for MD simulations. As with water simulations, comparison of simulations to the membrane dynamics measured with the 2D IR experiments provides a test of the accuracy of the simulations.

AUTHOR INFORMATION

Corresponding Author

fayer@stanford.edu

Present Address

[#]Department of Chemistry, Indiana University, Bloomington, Indiana 47405, United States.

Notes

The authors declare no competing financial interest.

ACKNOWLEDGMENTS

This work was funded by the Division of Chemical Sciences, Geosciences, and Biosciences, Office of Basic Energy Sciences of the U.S. Department of Energy through Grant #DE-FG03-84ER13251, and by the Division of Chemistry, Directorate of Mathematical and Physical Sciences, National Science Foundation Grant #CHE-1157772. A.T. thanks the Stanford Graduate Fellowship program for a research fellowship. O.K. thanks the Swiss National Science Foundation for a postdoctoral fellowship.

REFERENCES

(1) Janmey, P. A.; Kinnunen, P. K. J. *Trends Cell Biol.* **2006**, *16*, 538−546.
(2) Lee, A. G. *Biochim. Biophys. Acta* **2004**, *1666*, 62−87.
(3) Mcintosh, T. J.; Simon, S. A. *Annu. Rev. Biophys. Biomol. Struct.* **2006**, *35*, 177−198.
(4) Jensen, M. O.; Mouritsen, O. G. *Biochim. Biophys. Acta, Biomembr.* **2004**, *1666*, 205−226.
(5) Bienveniie, M.; Marie, J. S. *Curr. Top. Membr.* **1994**, *40*, 319−354.
(6) *Membrane Structure*, 3rd ed.; Seelig, A., Seelig, J., Eds.; Academic Press: New York, 2002.
(7) Cullis, P. R.; Fenske, D. B.; Hope, M. J. In *New Comprehensive Biochemistry*; Vance, D. E., Vance, J. E., Eds.; Elsevier Science: Amsterdam, 1996.
(8) McIntosh, T. J. *Curr. Top. Membr.* **1999**, *38*, 23−47.
(9) Lecuyer, H.; Dervichian, D. G. *J. Mol. Biol.* **1969**, *45*, 39−57.
(10) El-Sayed, M. Y.; Guion, T. A.; Fayer, M. D. *Biochemistry* **1986**, *25*, 4825−4832.
(11) Ladbrook, B. D.; Williams, R. M.; Chapman, D. *Biochim. Biophys. Acta* **1968**, *150*, 333−340.
(12) Calhoun, W. I.; Shipley, G. G. *Biochemistry* **1979**, *18*, 1717−1722.
(13) Needham, D.; Nunn, R. S. *Biophys. J.* **1990**, *58*, 997−1009.
(14) Demchenko, A. P.; Mély, Y.; Duportail, G.; Klymchenko, A. S. *Biophys. J.* **2009**, *96*, 3461−3470.
(15) Saxton, M. J.; Jacobson, K. *Annu. Rev. Biophys. Biomol. Struct.* **1997**, *26*, 373−399.
(16) Lee, M.-T.; Chen, F.-Y.; Huang, H. W. *Biochemistry* **2004**, *43*, 3590−3599.
(17) Hu, W.; Webb, L. J. *J. Phys. Chem. Lett.* **2011**, *2*, 1925−1930.
(18) Pius, J.; Morrow, M. R.; Booth, V. *Biochemistry* **2012**, *51*, 118−125.
(19) Yan, E. C. Y.; Eisenthal, K. B. *Biophys. J.* **2000**, *79*, 898−903.
(20) Hubner, W.; Blume, A. *Chem. Phys. Lipids* **1998**, *96*, 99−123.
(21) Chiang, Y. W.; Costa, A. J.; Freed, J. H. *Appl. Magn. Reson.* **2007**, *31*, 375−386.
(22) Borbat, P. P.; Costa-Filho, A. J.; Earle, K. A.; Moscicki, J. K.; Freed, J. H. *Science* **2001**, *291*, 266−269.
(23) Marsh, D. *Biochim. Biophys. Acta, Biomembr.* **2010**, *1798*, 688−699.
(24) Marsh, D.; Kurad, D.; Livshits, V. A. *Magn. Reson. Chem.* **2005**, *43*, S20−S25.
(25) Subczynski, W. K.; Widomska, J.; Feix, J. B. *Free Radical Biol. Med.* **2009**, *46*, 707−718.
(26) Filippov, A.; Orädd, G.; Lindblom, G. *Biophys. J.* **2008**, *84*, 3079−3086.
(27) Veatch, S. L.; Soubias, O.; Keller, S. L.; Gawrisch, K. *Proc. Natl. Acad. Sci. U. S. A.* **2007**, *104*, 17650−17655.
(28) Kurze, V.; Steinbauer, B.; Huber, T.; Beyer, K. *Biophys. J.* **2008**, *78*, 2441−2451.
(29) Schreier-Muccillo, S.; Marsh, D.; Dugas, H.; Schneider, H.; Smith, I. C. P. *Chem. Phys. Lipids* **1973**, *10*, 11−27.
(30) Chiang, Y. W.; Costa, A. J.; Freed, J. H. *J. Phys. Chem. B* **2007**, *111*, 11260−11270.
(31) Livshits, V. A.; Kurad, D.; Marsh, D. *J. Phys. Chem. B* **2004**, *108*, 9403−9411.
(32) Subczynski, W. K.; Wisniewska, A.; Hyde, J. S.; Kusumi, A. *Biophys. J.* **2007**, *92*, 1573−1584.
(33) Smirnov, A. I.; Smirnov, T. I.; Morse, P. D. *Biophys. J.* **1995**, *68*, 2350−2360.
(34) Park, S.; Kwak, K.; Fayer, M. D. *Laser Phys. Lett.* **2007**, *4*, 704−718.
(35) Kumar, K. S. K.; Tamimi, A.; Fayer, M. D. *J. Chem. Phys.* **2012**, *137*, 184201.
(36) Moilanen, D. E.; Fenn, E. E.; Wong, D.; Fayer, M. D. *J. Chem. Phys. B* **2009**, *131*, 014704.
(37) Woys, A. M.; Lin, Y.-S.; Reddy, A. S. X., Wei; de Pablo, J. J.; Skinner, J. L.; Zanni, M. T. *J. Am. Chem. Soc.* **2010**, *132*, 2832−2838.
(38) Manor, J.; Mukherjee, P.; Lin, Y.-S.; Leonov, H.; Skinner, J. L.; Zanni, M. T.; Arkin, I. T. *Struct. Bonding (Berlin, Ger.)* **2009**, *17*, 247−254.
(39) Remorino, A.; Korendovych, I. V.; Wu, Y.; DeGrado, W. F.; Hochstrasser, R. M. *Science* **2011**, *332*, 1206−1209.
(40) Remorino, A.; Hochstrasser, R. M. *Acc. Chem. Res.* **2012**, *45*, 1896−1905.
(41) Volkov, V. V.; Chelli, R.; Muniz-Miranda, F.; Righini, R. *J. Phys. Chem. B* **2011**, *115*, 5294−5303.
(42) Chieffo, L. R.; Shattuck, J. T.; Pinnick, E.; Amsden, J. J.; Hong, M. K.; Wang, F.; Erramilli, S.; Ziegler, L. D. *J. Phys. Chem. B* **2008**, *112*, 12776−12782.
(43) Asbury, J. B.; Steinel, T.; Kwak, K.; Corcelli, S. A.; Lawrence, C. P.; Skinner, J. L.; Fayer, M. D. *J. Chem. Phys.* **2004**, *121*, 12431−12446.
(44) Asbury, J. B.; Steinel, T.; Stromberg, C.; Corcelli, S. A.; Lawrence, C. P.; Skinner, J. L.; Fayer, M. D. *J. Phys. Chem. A* **2004**, *108*, 1107−1119.
(45) Fecko, C. J.; Loparo, J. J.; Roberts, S. T.; Tokmakoff, A. *J. Chem. Phys.* **2005**, *122*, 054506.
(46) Fecko, C. J.; Eaves, J. D.; Loparo, J. J.; Tokmakoff, A.; Geissler, P. L. *Science* **2003**, *301*, 1698−1702.
(47) Rector, K. D.; Jiang, J.; Berg, M.; Fayer, M. D. *J. Phys. Chem. B* **2001**, *105*, 1081−1092.
(48) Ijäs, K.; Lönnfors, M.; Nyholm, T. K. M. *Biochim. Biophys. Acta, Biomembr.* **2013**, *1828*, 932−937.
(49) Wang, T.; Widanapathirana, L.; Zhao, Y.; Hong, M. *Langmuir* **2012**, *28*, 17071−17078.
(50) Vostrikov, V. V.; Hall, B. A.; Sansom, M. S. P.; Koeppe, R. E. *J. Phys. Chem. B* **2012**, *116*, 12980−12990.
(51) Mojumdar, S. S.; Ghosh, S.; Mondal, T.; Bhattacharyya, K. *Langmuir* **2012**, *28*, 10230−10237.

(52) Skar-Gislinge, N.; Simonsen, J. B.; Mortensen, K.; Feidenhans'l, R.; Sligar, S. G.; Moller, B. L.; Bjornholm, T.; Arleth, L. *J. Am. Chem. Soc.* **2010**, *132*, 13713−13722.
(53) Bennun, S. V.; Faller, R.; Longo, M. L. *Langmuir* **2008**, *24*, 10371−10381.
(54) Yu, M.; Urban, M. W.; Sheng, Y. H.; Leszczynski, J. *Langmuir* **2008**, *24*, 10382−10389.
(55) Umakoshi, H.; Morimoto, K.; Ohama, Y.; Nagami, H.; Shimanouchi, T.; Kuboi, R. *Langmuir* **2008**, *24*, 4451−4455.
(56) Cady, S. D.; Hong, M. *Proc. Natl. Acad. Sci. U. S. A.* **2008**, *105*, 1483−1488.
(57) Adams, D. R.; Toner, M.; Langer, R. *Langmuir* **2007**, *23*, 13013−13023.
(58) Bennun, S. V.; Longo, M. L.; Faller, R. *Langmuir* **2007**, *23*, 12465−12468.
(59) Rezler, E. M.; Khan, D. R.; Lauer-Fields, J.; Cudic, M.; Baronas-Lowell, D.; Fields, G. B. *J. Am. Chem. Soc.* **2007**, *129*, 4961−4972.
(60) Corvis, Y.; Barzyk, W.; Brezesinski, G.; Mrabet, N.; Badis, M.; Hecht, S.; Rogalska, E. *Langmuir* **2006**, *22*, 7701−7711.
(61) Phang, T. L.; McClellan, S. J.; Franses, E. I. *Langmuir* **2005**, *21*, 10140−10147.
(62) Zhao, W.; Moilanen, D. E.; Fenn, E. E.; Fayer, M. D. *J. Am. Chem. Soc.* **2008**, *130*, 13927−13937.
(63) Ghosh, A.; Smits, M.; Bredenbeck, J.; Muller, M.; Bonn, M. *J. Am. Chem. Soc.* **2007**, *129*, 9608−9609.
(64) Piatkowski, L.; de Heij, J.; Bakker, H. J. *J. Phys. Chem. B* **2013**, *117*, 1367−1377.
(65) Gruenbaum, S. M.; Skinner, J. L. *J. Chem. Phys. C* **2011**, *135*, 075101.
(66) Gruenbaum, S. M.; Pieniazek, P. A.; Skinner, J. L. *J. Chem. Phys. C* **2011**, *135*, 164506.
(67) Metzler, D. E. *Biochemistry: The Chemical Reactions of Living Cells*, 2nd ed.; Harcourt/Academic Press: San Diego, 2001.
(68) Nagle, J. F.; Tristram-Nagle, S. *Biochim. Biophys. Acta, Rev. Biomembr.* **2000**, *1469*, 159−195.
(69) Tristram-Nagle, S.; Nagle, J. F. *Chem. Phys. Lipids* **2004**, *127*, 3−14.
(70) Milhaud, J. *Biochim. Biophys. Acta* **2004**, *1663*, 19−51.
(71) Kwak, K.; Park, S.; Finkelstein, I. J.; Fayer, M. D. *J. Chem. Phys.* **2007**, *127*, 124503.
(72) Kwak, K.; Rosenfeld, D. E.; Fayer, M. D. *J. Chem. Phys.* **2008**, *128*, 204505.
(73) Tokmakoff, A.; Urdahl, R. S.; Zimdars, D.; Francis, R. S.; Kwok, S.; Fayer, M. D. *J. Chem. Phys.* **1995**, *102*, 3919−3931.
(74) Tokmakoff, A.; Sauter, B.; Fayer, M. D. *J. Chem. Phys.* **1994**, *100*, 9035−9043.
(75) Williams, R. B.; Loring, R. F.; Fayer, M. D. *J. Phys. Chem. B* **2001**, *105*, 4068−4071.
(76) Merchant, K. A.; Noid, W. G.; Akiyama, R.; Finkelstein, I.; Goun, A.; McClain, B. L.; Loring, R. F.; Fayer, M. D. *J. Am. Chem. Soc.* **2003**, *125*, 13804−13818.
(77) Bagchi, S.; Nebgen, B. T.; Loring, R. F.; Fayer, M. D. *J. Am. Chem. Soc.* **2010**, *132*, 18367−18376.
(78) Petrache, H. I. *Comp. Biophys.* **2012**, *5*, 3−15.
(79) Petrache, H. I.; Tristram-Nagle, S.; Gawrisch, K.; Harries, D.; Parsegian, V. A.; Nagle, J. F. *Biophys. J.* **2004**, *86*, 1574−1586.
(80) Mashaghi, A.; Partovi-Azar, P.; Jadidi, T.; Nafari, N.; Maass, P.; Tabar, M. R. R.; Bonn, M.; Bakker, H. J. *J. Chem. Phys.* **2012**, 136.
(81) Meirovitch, E.; Freed, J. H. *J. Phys. Chem.* **1980**, *84*, 3281−3295.
(82) White, S. H.; King, G. I. *Proc. Natl. Acad. Sci. U. S. A.* **1985**, *82*, 6532−6536.
(83) Gawrisch, K.; Gaede, H. C.; Mihaela, M.; White, S. H. *Eur. Biophys. J. Biophys. Lett.* **2007**, *36*, 281−291.
(84) Meister, K. N., J.; Schatzschneider, U.; Metzler-Nolte, N.; Schmidt, D. A.; Havenith, M. *Angew. Chem. Int. Ed* **2010**, *49*, 3310−3312.
(85) Voon Kong, K.; Lam, Z.; Goh, W. D.; Leong, W. K.; Olivo, M. *Angew. Chem., Int. Ed.* **2012**, *51*, 9796−9799.
(86) Kumar, K. S. K.; Tamimi, A.; Fayer, M. D. *J. Am. Chem. Soc.* **2013**, *135*, 5118−5126.
(87) Kucerka, N.; Liu, Y.; Chu, N.; Petrache, H. I.; Tristram-Nagle, S.; Nagle, J. F. *Biophys. J.* **2005**, *88*, 2626−2637.
(88) Rapaport, H.; Kuzmenko, I.; Lafont, S.; Kjaer, K.; Howes, P. B.; Als-Nielsen, J.; Lahav, M.; Leiserowitz, L. *Biophys. J.* **2001**, *81*, 2729−2736.
(89) Simon, S. A.; McIntosh, T. J. *Methods Enzymol.* **1986**, *127*, 511−521.
(90) Simon, S. A.; Mcintosh, T. J.; Latorre, R. *Science* **1982**, *216*, 65−67.
(91) Mannock, D. A.; Lewis, R. N. A. H.; McMullen, T. P. W.; McElhaney, R. N. *Chem. Phys. Lipids* **2010**, *163*, 403−448.